Journal of Polymers and the Environment (2021) 29:588–598
https://doi.org/10.1007/s10924-020-01906-5

ORIGINAL PAPER

Preparation of Active Nanocomposite Film Consisting of Sodium Caseinate, ZnO Nanoparticles and Rosemary Essential Oil for Food Packaging Applications

Mahmood Alizadeh-Sani[1] · Ehsan Moghaddas Kia[2] · Zahra Ghasempour[3] · Ali Ehsani[3]

Accepted: 23 September 2020 / Published online: 29 September 2020

Abstract

Active films based on sodium caseinate (SC) were fabricated via the casting method; these films were reinforced with zinc oxide nanoparticles (ZnO NPs) and rosemary essential oil (REO). The films' optical, mechanical, and barrier and antimicrobial properties were evaluated. Further characterization was done using SEM, XRD, and FTIR spectroscopy. The results disclosed that the incorporation of ZnO NPs and REO into the SC matrix significantly improved the mechanical and barrier properties as well as moisture resistance of the SC film. The simultaneous incorporation of ZnO NPs and REO considerably reduced the water vapor permeability (WVP) of the films but increased their flexibility and strength. The microscopic and spectroscopic characterization revealed that the additives were highly compatible with the SC film matrix given the formation of uniform and homogeneous composite films. The nanocomposite films also exhibited noteworthy antimicrobial activity against the tested bacteria. In summary, this type of biopolymer-based active film can be considered as a promising material for food packaging applications.

Keywords Active packaging · ZnO nanoparticles · Rosemary essential oil · Nanocomposite · Biopolymeric material

Abbreviations

SEM	Scanning electron microscopy
XRD	X-ray diffraction
FTIR	Fourier transform infrared
WVP	Water vapor permeability
ZnO	Zinc oxide
NPs	Nanoparticles
SC	Sodium caseinate
REO	Rosemary essential oil

Introduction

In recent years, biopolymer-based food packaging films containing natural extracts have been increasingly considered by the food industry. Food packaging can be used to control the microbiological spoilage of food products, ensure food safety, increase durability, and reduce the associated environmental burden [1]. Currently, the utilization of biocompatible packaging materials and biopolymers has become much more widespread relative to petroleum-based, non-biodegradable, synthetic plastics [2]. Population growth and environmental dangers, as well as human health concerns, have led to the use of biodegradable polymers with non-toxic and environmentally friendly properties together with other biologically active natural products that improve food properties [3, 4]. In fact, nanocomposite films incorporated with nanoparticles (NPs) and natural essential oils/ or extracts feature antibacterial, antifungal, and antioxidant properties, improving the quality and durability of food products [5, 6]. Therefore, such natural biopolymers can be highly beneficial alternatives to synthetic, non-degradable materials.

In some cases, natural biopolymers have low mechanical resistance, presenting as a major limitation. Furthermore, although these materials have good film-forming properties,

✉ Ehsan Moghaddas Kia
ehsan.m.kia@gmail.com

✉ Ali Ehsani
ehsani@tbzmed.ac.ir

[1] Division of Food Safety and Hygiene, School of Public Health, Tehran University of Medical Science, Tehran, Iran

[2] Department of Food Science and Technology, Maragheh University of Medical Sciences, Maragheh, Iran

[3] Department of Food Science and Technology, Faculty of Nutrition and Food Sciences, Tabriz University of Medical Sciences, Tabriz, Iran

they are permeable to water vapor due to their hydrophilic properties. To overcome these defects, multiple compounds like proteins, polysaccharides, lipids, and their derivatives have been used in combination with each other or with other reinforcing materials and nanofillers to fabricate composite packaging materials [7, 8]. It should be noted that, biocompatible films based on proteins have more suitable mechanical resistance and barrier characteristics than those based on polysaccharides [9]. Therefore, to achieve desirable films, it is better to use a combination of these compounds [1, 7, 10]. In general, composite films have been prepared using various formulations, with protein compounds such as casein, whey protein, corn saddle, soy protein, wheat gluten, and gelatin often being utilized [11]. Sodium caseinate (SC) is one of the compounds that has been used to form biodegradable films and coatings; the encapsulation of bioactive compounds with SC has also been described in previous studies [7, 11, 12]. Notably, SC possesses satisfactory thermal stability and can easily produce transparent, flexible, colorless, eco-friendly films from aqueous solutions owing to its random coil nature and ability to form intermolecular bonds and make electrostatic and hydrophobic interactions [7, 9].

Essential oils (EOs) are volatile functional compounds derived from different parts of fragrant plants. These oils offer a wide range of applications as they are rich in terpenoids, terpenes, aromatics, and aliphatic compounds. In addition to their antimicrobial and antioxidant activity (main properties), these compounds provide a number of functional properties for active packaging films [7, 13]. Rosemary (*Rosmarinus officinalis*) essential oil (REO) is a well-known spice that has been successfully used in the fabrication of active packaging films owing to its antioxidant and antimicrobial properties [13, 14]. In fact, EOs can improve the moisture sensitivity and flexibility of such composite films due to their oily and hydrophobic nature [5, 7, 15].

In active packaging, antimicrobial NPs such as zinc, iron, gold, silver, and titanium dioxide are used in order to inhibit microbial growth, prolong product quality, and increase the shelf life of food products [7, 16]. Among the metal oxides, the antimicrobial properties of zinc oxide (ZnO) are exemplary, making it one of the most useful materials in this field. In fact, ZnO NPs can maintain product color and improve product quality for a long period besides boosting the mechanical properties of the packaging material. Furthermore, various studies have shown that the utilization of ZnO NPs along with other compounds such as chitosan, cellulose, protein, and their derivatives is suitable for improving film performance [1, 3, 16].

Therefore, in this study, functional nanocomposite films were prepared by incorporating ZnO NPs and REO into a SC matrix via the casting method. The composition, structure, and function of the products were characterized via SEM, FTIR, and XRD analyses. In addition, the effects of nanofillers and EOs on the morphological, physico-mechanical, water vapor barrier, and antimicrobial properties of the composite films were investigated.

Materials and Methods

Materials

ZnO NPs (> 99% purity; ~10–30 nm) were purchased from US Research Nanomaterials, Inc., Houston, (U.S.A). SC (protein > 90%) was purchased from Iran Caseinate (Tehran, Iran). REO was procured from the Barijessence Company (Kashan, Iran). All the applied reagents were of analytical grade and were used without further purification. Deionized water was used for all sample preparations. The bacterial strains including *Listeria monocytogenes* (ATCC 13932), *Escherichia coli* (ATCC 25922), *Staphylococcus aureus* (ATCC 33591) and *Pseudomonas fluorescens* (ATCC 13525) were obtained from the Biological and Genetic Resources Center (Tehran, Iran). The microbial culture media were acquired from Micromedia (Canada).

Preparation of SC And Nanocomposite Films

The SC solution was prepared at a concentration of 8% (w/v) in distilled water at pH = 8; the pH was adjusted slowly using NaOH over 2 h. Then, the solution was heated in a water-bath at 90 °C for 30 min. Glycerol (4.5% w/w), as a plasticizer, was added to the SC solution before it was degassed under vacuum. In the next step, an Ultrasonic Cleaner (Belfor, U.S.A) was applied for 30 min at 25 °C to remove any trapped air bubbles. The solution films were poured and spread on a petri dish with 8 cm internal diameter and then dried for 24 h in a vacuum oven set at 30 ± 1 °C and 50 ± 6% relative humidity (RH).

Various amounts of ZnO NPs (0.5, 1 and 2% w/w based on SC) were added to the SC film solutions. To obtain good dispersion in the film solution, the ZnO NPs were added slowly under intense stirring, with an ultrasonic probe sonicator (UCD-1200 model, Bio-Base, China) being used simultaneously. Finally, REO was added with concentrations of 1% and 2% (w/v based on SC) to the composite film solutions, and the solutions were completely homogenized using Ultra-Turrax (IKA. Germany) homogenizers for 10 min at 5000 rpm. The film suspensions containing the dispersed ZnO NPs and REO were cast onto petri dishes with 8 cm internal diameter and then dried for 24 h using a vacuum oven set at 30 ± 1 °C and 50 ± 6% RH. All dried films were peeled and stored at 25 ± 1 °C and 50 ± 6% RH ahead of further testing.

Antimicrobial Properties of Films

The antimicrobial properties of the films were determined by adapting the disc diffusion method [17]. After 18–24 h of growth in Mueller Hinton broth, the bacterial suspensions were collected. These bacterial samples were then adjusted to 0.5 McFarland standard turbidity (~1.5×10^8 CFU/mL). Then, serial dilutions were performed twice (1:10) to achieve a final bacterial density of ~1.5×10^6 CFU/mL. Subsequently, circular film samples (10 mm) were cut under sterile conditions and placed on Mueller-Hinton agar, which were inoculated with 0.1 mL of bacterial suspension (~1.5×10^6 CFU/mL). The samples were incubated for 24 h at 25 °C for *P. fluorescens* and at 37 °C for the remaining strains. A digital micrometer was finally used to measure the zone of inhibition surrounding each disc.

Physical Properties

Film Transparency

The transparency of the films was measured at a selected wavelength (600 nm) using a UV–Vis recording spectrophotometer (Unico, UV-2100, USA) according to ASTM D1746-09 [18].

Moisture Content

The moisture content (MC) of the composite films was measured according to the films' variation in weight after drying in a laboratory oven at 105 ± 1 °C until a constant weight was achieved (dry sample weight). Measurements were performed with three replications for each film, facilitating the calculation of the MC.

Moisture Absorption

For determination of the amount of moisture absorption (MA) in the films, dried films with the dimensions of 20 × 20 mm and 0% RH were kept for 24 h and then weighed. Next, these films were transferred to a desiccator containing saturated calcium nitrite in order to boost the RH to 55%. Weighing was performed at regular intervals until an equilibrium state was achieved.

Water Solubility

The samples were dried at 50 °C for 5 h in a laboratory oven, before being weighed then immersed in 40 mL of distilled water for 24 h at ambient temperature. Then, the remains of the film were filtered and dried at 110 °C for 7 h to determine the weight of the final matter that had not dissolved in the water. The percentage of water solubility (WS) was determined by comparing the initial dry matter with the remaining dry matter.

Water Vapor Permeability

Water vapor permeability (WVP) was determined according to the ASTM E-96 standard [19] through a modified procedure. The films were sealed in a glass permeation cup (8 mm diameter). To create 100% RH inside the films, the cups were filled with calcium chloride dehydrate and placed in desiccators containing distilled water. The cups were weighed every 3 h over a 48-h period. The WVP (g. m/m^2. s. Pa) was calculated according to the following Eq. (1):

$$\mathrm{WVP} = \frac{\mathrm{D} \bullet \mathrm{X}}{\mathrm{A} \bullet \Delta \mathrm{P}} \tag{1}$$

where D is the transmission rate of water vapor (g/s), X is the film thickness (m), A is the area of exposed film (m^2) and ΔP is the water vapor pressure difference across the film (Pa).

Film Thickness

The thickness of each film was determined using a digital micrometer (Mitutoyo, Japan) with an accuracy of 0.001 mm. The measurements were made randomly at five points. The mean film thickness was used in the determination of other physical and mechanical properties.

Mechanical Properties

The tensile strength (TS), Young's modulus (YM) and elongation at break (EB) of the films were evaluated with a texture analyser (Microelectronics Universal Testing Instrument Model DBBP-20, Bongshin, Korea). The film samples were cut into 10 × 1 cm pieces. An initial grip separation of 50 mm and a crosshead speed of 10 mm/min at 25 °C were applied. The equations below were used to calculate the mentioned parameters.

$$\text{Tensile strength (MPa)} = \frac{\text{Load at break}}{\text{Original width} \times \text{Original thickness}} \tag{2}$$

$$\text{Percent elongation (\%)} = \frac{\text{Elongation at rupture}}{\text{Initial gauge length}} \times 100 \tag{3}$$

$$\text{Young's modulus (MPa)} = \frac{(\text{Load at point on tangent} \,/ \text{Original width} \times \text{Original thickness})}{\text{Elongation at point on tangent} \,/\, \text{Initial gauge length}} \tag{4}$$

Characterization of the Films

Scanning Electron Microscopy

The surface and cross-sectional morphology of the films were observed by scanning electron microscopy (SEM) model TESCAN MIRA 3 XMU (Czech Republic). Before scanning, the films were coated with a thin layer of gold; an accelerating voltage of 20 kV was applied.

X-ray Diffraction

The X-ray diffraction (XRD) patterns of the films were recorded using an X-ray diffractometer (PANalytical X′pert pro MRD diffractometer, Amsterdam, Netherlands). The nickel-filtered Cu Kα radiation beam of the device was applied in the angular range of 10 to 80 (2θ) at 40 kV voltage with 30 mA current.

Fourier Transform Infrared Spectroscopy

The Fourier transform infrared (FTIR) spectra of the films were obtained using a Bruker Tensor 27 FTIR spectrophotometer (Bruker, Germany). The spectra were acquired in the Attenuated Total Reflectance (ATR) mode between 4000–400 cm^{-1} across 16 scans at a resolution of 4 cm^{-1} for each sample.

Statistical Analysis

All statistical analyses were performed in the SPSS software (SPSS Inc., IBM; Armonk, N. Y, USA). One-way analysis of variance (ANOVA) was employed to assess significant differences, with further analysis of significant results being done via the Tukey multiple range post hoc tests ($P < .05$). The values were reported as mean ± standard deviation (SD); all tests were performed in triplicates.

Results and Discussion

Antimicrobial Activity

The ability of packaging materials to inhibit the bacterial spoilage of foods or growth of pathogenic bacteria is a desirable functional attribute. Hence, a disc diffusion test was utilized to assess the antibacterial activities of the nanocomposite films (Table 1). As expected, the SC film showed no inhibitory effect against the various bacteria studied. The antibacterial efficacy of the composite films depended on the concentration and type of materials present. Interestingly, the films containing a combination of ZnO NPs and REO exhibited stronger antimicrobial activity than those containing either of these antimicrobial agents. This effect may have been because the combination exhibited synergism as the two substances had differing mechanisms of action [20]. Overall, the nanocomposite films appeared to be more effective against Gram-positive bacteria (especially *L. monocytogenes*) than Gram-negative ones (*E. coli*), which suggests that the nature of the microbial cell wall was an important factor. It is possible that the NPs disrupted the microbial cell membrane properties, thereby having an adverse effect on key biochemical processes, such as transmembrane transport, DNA replication, and protein synthesis [21, 22]. In addition, the essential oils and NPs can generate reactive oxygen species (ROS) that can damage phospholipid molecules present in the cell membrane [23, 24]. Our findings are consistent with those reported by other researchers on the impact of composite films on microbial activity [21].

Table 1 Antimicrobial activity of nanocomposite film containing ZnO, REO and ZnO/REO

	Diameter of inhibition zone (mm)		
	1%ZnO	2%REO	1%ZnO/2%REO
Bacteria strains	Mean ± SD	Mean ± SD	Mean ± SD
L. monocytogenes	13.00 ± 0.55^{a}	15.30 ± 0.55^{d}	15.80 ± 0.35^{g}
S. aureus	13.50 ± 0.68^{a}	14.50 ± 0.51^{b}	15.50 ± 0.15^{g}
E. coli	11.20 ± 0.52^{b}	13.50 ± 0.60^{e}	13.40 ± 0.26^{h}
P. fluorescence	10.90 ± 0.70^{b}	12.60 ± 0.90^{f}	12.70 ± 0.37^{c}

REO rosemary essential oil, *ZnO NPs* zinc oxide nanoparticles

The values are presented as mean ± standard deviation. Any two means in the same column followed by the same letter are not significantly ($P > 0.05$) different.

Physical Properties

Transparency

Film transparency is influenced by the film matrix ingredients and exerts a major impact on the consumer acceptance of packaged products [25]. Based on the results (Table 2), the SC film had the maximum transparency among all samples. By increasing the amounts of REO and ZnO NPs, the transparency of the films decreased significantly ($P < .05$). The addition of ZnO NPs reduced the transparency more relative to REO addition. A good explanation for this observation is the mineral nature of the ZnO NPs. However, the reduction in transparency was dependent on the type of and concentrations of the materials [17, 26]. Furthermore, the simultaneous addition of ZnO NPs and REO significantly reduced film transparency due to synergistic effects between the compounds and the matrix, with non-uniform distributions of the NPs and even REO at high concentrations [17]. On the other hand, the reduced transparency observed in

Table 2 The physical properties of SC film combined with ZnO NPs and REO

Films	WVP ($\times 10^{-11}$ g.m/m^2. s. Pa)	Moisture content (%)	Water solubility (%)	Moisture absorption (%)	T600 (%)
	Mean ± SD	Mean ± SD	Mean ± SD	Mean ± SD	Mean ± SD
SC	1.46 ± 0.00^{a}	12.35 ± 0.003^{ab}	43.33 ± 0.057^{a}	20.16 ± 0.002^{ac}	70.53 ± 0.04^{a}
SC/1%REO	1.20 ± 0.004^{ab}	10.24 ± 0.007^{b}	39.60 ± 0.001^{b}	12.33 ± 0.001^{b}	61.36 ± 0.05^{b}
SC/2%REO	1.18 ± 0.001^{ac}	10.71 ± 0.007^{c}	38.67 ± 0.005^{c}	12.46 ± 0.003^{b}	56.73 ± 0.02^{c}
SC/0.5%ZnO	1.23 ± 0.002^{ab}	11.68 ± 0.001^{d}	37.46 ± 0.005^{d}	16.68 ± 0.001^{c}	51.90 ± 0.03^{d}
SC/1%ZnO	1.14 ± 0.001^{d}	11.03 ± 0.005^{e}	36.30 ± 0.004^{e}	13.31 ± 0.002^{d}	46.63 ± 0.02^{e}
SC/2%ZnO	1.29 ± 0.000^{e}	11.35 ± 0.003^{f}	35.16 ± 0.001^{ab}	14.19 ± 0.000^{e}	45.83 ± 0.04^{f}
SC/0.5%ZnO/1%REO	1.25 ± 0.00^{ab}	10.41 ± 0.004^{ac}	37.16 ± 0.002^{d}	12.90 ± 0.001^{f}	45.43 ± 0.03^{f}
SC/0.5%ZnO/2%REO	1.22 ± 0.005^{ab}	10.35 ± 0.008^{ac}	37.33 ± 0.003^{d}	14.39 ± 0.005^{e}	46.93 ± 0.02^{e}
SC/1%ZnO/1%REO	1.35 ± 0.005^{c}	10.06 ± 0.005^{bc}	34.23 ± 0.003^{bc}	16.72 ± 0.004^{c}	43.70 ± 0.06^{ab}
SC/1%ZnO/2%REO	1.31 ± 0.003^{c}	11.33 ± 0.000^{f}	33.13 ± 0.001^{ad}	13.28 ± 0.002^{d}	43.30 ± 0.01^{ab}
SC/2%ZnO/1%REO	1.28 ± 0.005^{ad}	11.41 ± 0.006^{f}	30.20 ± 0.002^{f}	10.65 ± 0.006^{ab}	42.80 ± 0.05^{f}
SC/2%ZnO/2%REO	1.33 ± 0.001^{c}	10.78 ± 0.001^{bd}	28.66 ± 0.001^{g}	10.23 ± 0.002^{ab}	42.23 ± 0.07^{f}

Statistical analysis reported based on ANOVA test

P value considered less than 0.05 vs. control group

SC sodium caseinate, *ZnO* zinc oxide, *REO* rosemary essential oil, *T* transparency

the ZnO-based films is mostly due to the prevention of light transmission by the light-impermeable ZnO NPs [27].

Moisture Content

The MC of a film provides an indication of the amount of water it can absorb and incorporate into its internal structure [28]. As depicted in Table 2, the incorporation of the ZnO NPs and REO into the SC films decreased their MC. In fact, the MC of the SC films was around 12.35%, whereas this value was 10.71% and 11.35% for the films containing 2% REO or 2% ZnO NPs, respectively. Arfat et al. [26], reported that such a decrease in the MC of polymer films can be attributed to the ability of NPs to fill some pores of the films in addition to the hydrophobic nature of the REO.

Moisture Absorption

The MA values of the SC films containing different concentrations of REO and ZnO NPs are shown in Table 2. Based on the results, the MA of the SC film decreased significantly with the addition of different concentrations of REO and ZnO NPs ($P < .05$). These changes in MA are usually attributed to the hydrophobic nature of ZnO NPs and REO, as well as decreased intermolecular interactions between water and essential oil molecules in the film matrix [29, 30]. The MA amount of the SC film was 20.16%, while the blended film containing 2% REO/2% ZnO NPs had the lowest MA value at about 10.23% ($P < .05$). ZnO NPs, with low hydrophilicity, can reduce the MA values of SC films. Furthermore, the establishment of a network structure by the combination of REO and ZnO NPs amplifies the water resistance and can deter water molecules from assimilating into nanocomposite films [31].

Water Solubility

A biodegradable film should form a protective coating around a food product throughout its lifetime but subsequently degrade when it is released into the environment [32]. The values of WS are conveyed in Table 2. The highest level of WS (43.33%) was seen in the SC film. However, the WS significantly declined with the incorporation of REO and ZnO NPs into the film matrix ($P < .05$). Boosting the presence of ZnO NPs in the composite film from 1% to 2% significantly reduced the WS from 34.23 to 28.66% ($P < .05$). The use of glycerol as a hydrophilic plasticizer increases the flexibility and water solubility of polymer films [33]. The strong connection of the ingredients to the nanocomposite film's matrix was responsible for the decline in WS [34]. Also, the dimensional ratio and tendency toward crystallization of additives (e.g., ZnO NPs and REO) are significant agents affecting the water resistance of nanocomposite films [15].

Water Vapor Permeability

WVP is one of the most important functional properties of food packaging films for maintenance of quality through minimal moisture conduction [15] between the ingredients and the surrounding atmosphere [35]. The lowest possible amount of WVP is desired for edible films [33]. Table 2

displays the role of different concentrations of REO and ZnO NPs added individually and in combination to the SC-based films. The results demonstrated the considerable impact of the concentrations of ZnO NPs and REO on WVP of the films. In fact, the WVP decreased with the incorporation of the additives in the SC film, especially when ZnO NPs and REO were added simultaneously. The SC biopolymer has a weak inhibitory effect on WVP (nearly 1.46×10^{-11} g.m/m^2.s.Pa); the reinforcement of the SC film with 2% REO or 2% ZnO NPs decreased this WVP to 1.18×10^{-11} g.m/m^2.s.Pa and $1.29 \times {}^{10-11}$ g.m/m^2.s.Pa, respectively. The results also showed that the addition of 2% ZnO NPs/2% REO significantly reduced the WVP of the SC film to 1.33×10^{-11} g.m/m^2.s.Pa ($P < .05$). These results are in accordance with the findings of several research regarding different nanocomposites [15, 26, 27, 36, 37]. The more hydrophobic nature of ZnO NPs relative to the SC film, the low aspect ratio of these NPs, and the formation of irregular chains led to the significant reduction in WVP [26]. Also, the combination of ZnO NPs and REO in the SC matrix resulted in a structure with complex pathways that hindered the permeation of water vapor [27]. Furthermore, the incorporation of REO into the SC film reduced the adsorption and permeability of water vapor due to increased hydrophobicity. The hydrophobic nature of REO is accounted by the presence of terpenes and terpenoids in its composition. Water vapor transfer becomes limited as the dispersed hydrophobic phase increases relative to the hydrophilic phase in protein films [9, 38]. Overall, the ZnO NPs and REO significantly improved the efficacy of the SC films for food packaging applications in terms of WVP.

Film Thickness

The thickness of the SC-based film is a factor that was influenced by the incorporation of the two additives in the polymer matrix. As shown in Table 3, the addition of REO to the film matrix increased the thickness of the edible film at an insignificant level. In contrast, the addition of ZnO NPs enhanced the thickness significantly ($P < .05$). The thickness of the SC film was 0.086 mm, whereas the thickness of the SC films containing 2% ZnO NPs (0.100 mm) or 2% REO/2% ZnO NPs (0.103 mm) were considerably higher ($P < .05$). In fact, the addition of fillers to various layers of a film's polymer network increases its solid content and thickness. These findings are in agreement with those of previous research [15, 36].

Mechanical Properties

The variation in mechanical properties of the films (tensile strength, Young's modulus and elongation at break) with the incorporation of ZnO NPs and REO at different concentrations (equilibrated at 55% RH and 25 °C) is presented in Table 3. The TS and YM values for the SC film were 4.32 MPa and 37.34%, respectively. Various percentages of ZnO NPs (0.5%, 1% and 2%) and REO (1% and 2%) were added to the SC film, as summarized in Table 3. The results elucidated that the incorporation of 0.5% ZnO NPs had no significant effect on the TS but significantly augmented the YM and EB values of the SC film ($P < .05$). When this concentration was boosted to 1%, the TS value reached 3.74 MPa while the YM value dropped to 17.31 MPa ($P < .05$). These behaviors might be associated with the

Table 3 The mechanical properties of SC film combined with ZnO NPs and REO

Films	Tensile strength (MPa) Mean ± SD	Elongation at break (%) Mean ± SD	Young's modulus (MPa) Mean ± SD	Thickness (mm) Mean ± SD
SC	4.32 ± 0.04^{a}	12.69 ± 0.04^{a}	37.34 ± 0.05^{a}	0.086 ± 0.002^{a}
SC/1%REO	3.96 ± 0.05^{b}	36.01 ± 0.03^{b}	13.81 ± 0.02^{b}	0.090 ± 0.001^{ab}
SC/2%REO	2.54 ± 0.03^{c}	33.74 ± 0.01^{c}	10.71 ± 0.02^{c}	0.090 ± 0.004^{ab}
SC/0.5%ZnO	4.31 ± 0.05^{a}	24.16 ± 0.05^{ab}	17.91 ± 0.03^{d}	0.091 ± 0.001^{ab}
SC/1%ZnO	4.74 ± 0.04^{d}	21.81 ± 0.03^{d}	17.31 ± 0.01^{e}	0.095 ± 0.003^{b}
SC/2%ZnO	4.37 ± 0.02^{a}	27.35 ± 0.02^{e}	16.02 ± 0.04^{f}	0.100 ± 0.007^{c}
SC/0.5%ZnO/1%REO	3.97 ± 0.03^{b}	10.40 ± 0.06^{ab}	17.92 ± 0.01^{d}	0.092 ± 0.005^{ab}
SC/0.5%ZnO/2%REO	3.12 ± 0.01^{ab}	18.05 ± 0.04^{ac}	17.86 ± 0.06^{d}	0.092 ± 0.002^{ab}
SC/1%ZnO/1%REO	2.18 ± 0.04^{e}	16.88 ± 0.05^{f}	17.08 ± 0.07^{ab}	0.096 ± 0.001^{d}
SC/1%ZnO/2%REO	2.09 ± 0.02^{e}	16.85 ± 0.01^{f}	16.38 ± 0.03^{g}	0.097 ± 0.005^{d}
SC/2%ZnO/1%REO	2.67 ± 0.05^{ac}	18.80 ± 0.03^{g}	14.35 ± 0.06^{h}	0.101 ± 0.003^{c}
SC/2%ZnO/2%REO	3.17 ± 0.01^{ab}	14.97 ± 0.04^{bc}	23.01 ± 0.05^{bd}	0.103 ± 0.006^{f}

Statistical analysis reported based on ANOVA test

SC Sodium caseinate, *ZnO* zinc oxide, *REO* Rosemary essential oil

P value considered less than 0.05 vs. control group

more compressed structure of these nanocomposites compared with the SC film. Furthermore, such improvements in mechanical properties could be ascribed to the suitable compatibility between the SC biopolymer and the ZnO NPs due to unique interactions (e.g., hydrogen bonding between Zn ions and the functional groups of SC) that lead to a uniform dispersion of the NPs [33, 39, 40]. When the concentration of the NPs was increased to 2%, the TS and EB increased even further, though the YM value fell. This drop in YM could be attributed to the slight agglomeration of the nanofillers (ZnO), inappropriate distribution of the NPs at higher contents, increased mobility of the chains, and damage to the network structure of the composite films by the large ZnO agglomerates [39, 41] that are clearly illustrated in the SEM images. Moreover, the decrease in TS of the nanocomposites compared with the pure polymer may be attributed to weak interfacial interactions between the ZnO NPs and SC matrix. It should also be noted that the strain-induced crystallization phenomenon plays an important role in the stability of polymers against strain localization and fracture formation [42]. Therefore, NPs, as hard, non-homogeneous particles, can reduce the resistance of a polymer matrix against fracture. The increased flexibility of the nanocomposite may be due to the formation of new mechanisms of energy dissipation in the presence of NPs [43]. These include the mechanism for cluster breakage, the phenomenon of the formation of micropores at the interface, the changes in the path of crack growth, and the transformation of the matrix shape. The tension that causes fracture is less than the tension created by the structure of the pure polymer. Hence, the formation of tiny clusters facilitates crack formation and, as a result, creates more gaps that play positive roles in the energy dissipation and ductility mechanisms. When the size of the NPs grows and the clusters are formed, the area of the polymer/NPs interface decreases. Therefore, the critical stress for the separation of the polymer/NPs fraction also decreases; this can be the reason for reaching an optimum level of ductility and minimizing flexibility at higher levels of the NPs [44]. Generally, the clustering of NPs at higher levels results in weakened mechanical and barrier properties of the polymer in comparison with lower levels of the NPs. Arfat et al. [26], in agreement with our study, reported that NPs reduced the TS of protein films at high concentrations. On the contrary, the addition of REO to the SC film led to different results. The SC films containing REO had higher EB but lower TS and YM compared with the SC film, regardless of the presence of ZnO NPs ($P < .05$). As a result, it should be considered that the addition of REO to the film mixture increased the heterogeneity of the films, reduced the rigidity and strength of the films, and increased the occurrence of irregularities in the structure of the biopolymer network. Since the main interactions occurring in protein films are comprised of hydrogen, carboxyl and sulfhydryl bonds [26, 33], the addition of an essential oil (e.g., REO) into protein-based films may decrease the interactions that occur between the protein chains [45]. According to many studies that have recommended essential oils (e.g., REO) as plasticizers, these compounds can penetrate into biopolymer matrices, increasing the volume of empty spaces in the biopolymer networks and reducing the strength of the interamolecular forces [26]. A number of studies have shown that the addition of essential oils or lipids at high concentrations reduces the TS of protein-based films [46]. The simultaneous addition of REO and ZnO NPs to SC films caused significant mechanical changes; these films had higher EB but lower TS and YM ($P < .05$). Thereby, the TS and YM for the SC/2%ZnO NPs/2%REO biocomposite film were 3.17 MPa and 23.01 MPa, respectively, while, the EB was 14.97%. These behaviors are usually related to the reinforcing effects of ZnO NPs on the biopolymer matrix due to their high surface energy and strong interfacial interactions with the polymer compounds, improving the mechanical properties of the polymer films [37]. It is generally known that the distribution, internal density, and intra-molecular interactions within the polymer matrix determine the mechanical properties of the film. The tensile test results demonstrate that the fabricated nanocomposite film had less strength and stiffness but greater flexibility relative to the protein film, suggesting the induction of structural changes in the protein after the incorporation of NPs. Rouhi et al. (2013) and Arfat et al. (2014) reported corresponding results in gelatin-based films and fish protein isolate/fish skin gelatin film, respectively. Thus, the incorporation of both ZnO NPs and REO into the SC film directly affects and develops its mechanical properties.

Characterization of SC Based-Films

Scanning Electron Microscopy

The obtained SEM micrographs of the cross sections and surface of the SC film and films containing ZnO NPs and REO are illustrated in Fig. 1. The images reveal that the films made of pure SC had homogeneous and smooth surfaces without any roughness or cracks, indicating proper mixing of the compounds. On the other hand, the remaining films had heterogeneous surfaces and small aggregates in the presence of ZnO NPs. According to the results of the SEM images, films containing ZnO NPs had a granular structure; however, significant accumulation was not observed in low concentrations of ZnO NPs (0.5% and 1%), indicating the homogeneity and suitable dispersion of inorganic NPs at low concentrations in the protein matrix. Nevertheless, after increasing the concentration of ZnO NPs to 2%, significant aggregation was observed at the film surface as ZnO NPs tend to cluster at high concentrations. At low concentrations, the size of these NPs was in the range of 10–30 nm, but

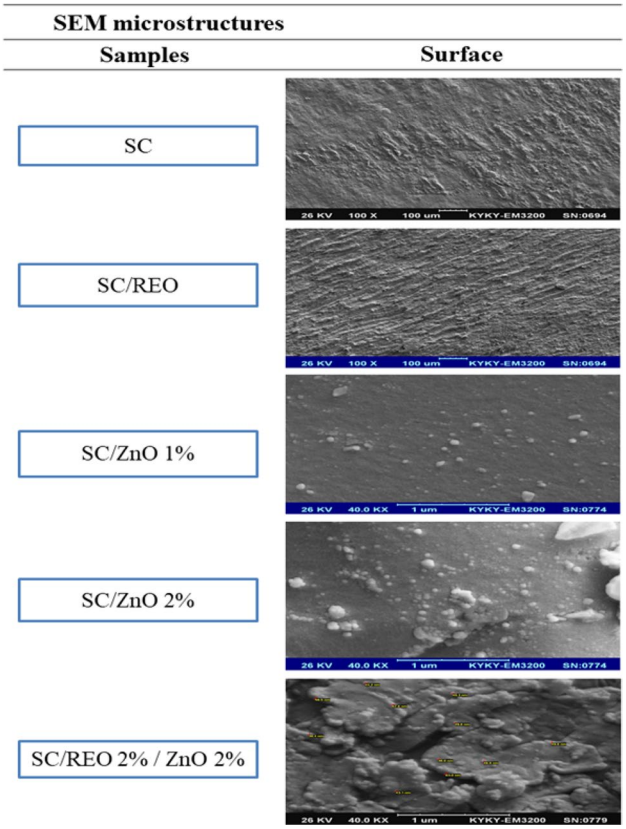

Fig. 1 SEM micrographs of surface of SC film combined with ZnO NPs and REO

50–100 nm clusters were observed at the higher concentration level. The clustering of the NPs can affect the properties of the nanocomposites as well as the boundary properties (permeability) of the resulting film. The granular morphology of the SC/2% ZnO film is demonstrated in the SEM image shown in Fig. 1, suggesting the presence of crystalline grains of ZnO NPs, in good agreement with the results of XRD. Increased phase discontinuity and stronger presence of agglomerates and aggregates could be clearly observed in the microstructure as the concentration of ZnO NPs was increased. A similar impact of ZnO NPs on the properties of protein films has been reported by Arfat et al. [26].

X-ray Diffraction (XRD)

The XRD patterns of the pure ZnO NPs and the SC film containing ZnO NPs and REO are presented in Fig. 2. According to the resulting patterns, ZnO NPs had significant peaks at 2θ = 31.5, 34.4, 36.3, 47.5, 56.6, 62.8, 66.4, 68, and 69.15°. Based on the Debye-Scherrer equation ($\tau = \kappa\,\lambda/\beta\,cos\theta$), the average crystallite size of the ZnO NPs was reported approximately between 20-100 nm. In this equation, τ is the mean crystalline size, κ is the shape factor constant (about 0.9), λ is the wavelength of X-ray radiation, β is the full width at half the maximum intensity (FWHM), and θ is the Bragg diffraction angle [39]. Considering that the size of the ZnO NPs were 20 nm before incorporation into the SC film, the larger size of the particles observed in the ZnO NPs/SC films can be attributed to the agglomeration and aggregation of the NPs in the protein matrix and the tendency of the NPs toward clustering at high concentrations [47]. Despite the presence of SC in the structure of the composite films, the crystalline structure of ZnO did not change, and the XRD patterns of the bionanocomposite films containing different amounts of ZnO revealed the same ZnO pattern. As shown in Fig. 2, the intensity of the ZnO peaks depended on the ZnO content and the presence of other compounds in the composite film. Reducing the concentration of ZnO NPs and adding REO decreased the intensity of the peaks, while the angle of diffraction of the films did not alter when changing the ZnO concentration. Decreased peak intensities in composite films are usually attributed to good miscibility between the crystalline and non-crystalline components [39]. Since SC comprised the majority of the film matrix in all of the bionanocomposite

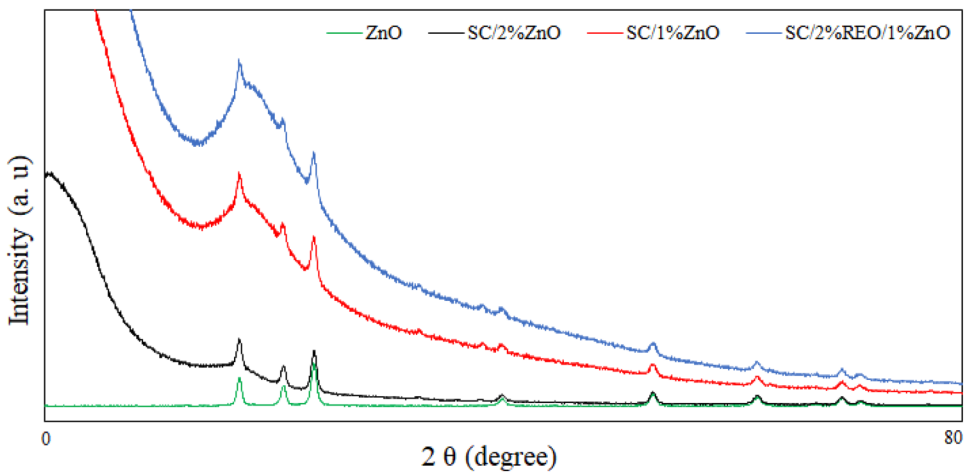

Fig. 2 XRD spectra of SC film combined with ZnO NPs and REO

films, similar patterns of XRD were detected with different ZnO levels, with only the peak intensities varying.

FTIR Spectroscopy

The FTIR analysis was conducted for identification of the functional groups and the interactions occurring between the components of the composite film, the results of which are illustrated in Fig. 3. Peaks situated at the wavenumbers of ~670, ~1035, ~1528, ~1640, ~2930, and ~3450 cm^{-1} were roughly present across all films. All samples displayed a major band at ~1700 cm^{-1}, which is the characteristic peak of amide-I and represents C = O stretching/bonding coupled with a COO group [26, 48]. The peak at ~1542 cm^{-1} is attributed to amide-II, arising from the bending vibrations of N–H groups and the stretching vibrations of C–N groups. The characteristic peaks of ZnO that were seen in the pure ZnO disappeared after it was combined with SC in the composite film [48, 49]. A broad band centered at 3000–3600 cm^{-1} is related to the -OH group and intermolecular hydrogen bonding. Therefore, the peaks at 3443 cm^{-1} in the spectra are due to the bending vibration and stretching of the –OH groups and the N–H stretching of the amide-A band coupled with hydrogen bonding [50]. Also, the amide-A band from the N–H stretching vibration of the hydrogen-bonded N–H group became more intense at wavenumbers around ~3600 cm^{-1} after incorporation of ZnO into the SC film. The greater intensity in the amide-A region proposes that N–H groups of the protein chain interacted with ZnO via hydrogen bonding [51]. Spectral changes were observed after addition of REO to the SC film; the broadness of the spectrum increased in the wavelength range of 3600 to 3000 cm^{-1}, elucidating the formation of hydrogen bonds between SC and REO considering the presence of hydroxyl groups in the rosemary structure. These phenomena are typically associated with the protein/REO interaction and the enfoldment of the components by the protein, such that the peaks at the area of ~3443 cm^{-1} are the widest [17]. Nevertheless, the incorporation of REO and ZnO into the SC film induced alterations in the intramolecular interactions and molecular structure of the matrix.

Conclusion

In this study, nanocomposite films were fabricated by embedding REO (as an antimicrobial and antioxidant) and ZnO NPs (as an antimicrobial, antioxidant and filler) within the SC matrix via casting. It was revealed that ZnO NPs and REO could improve the efficacy of the SC packaging by enhancing its mechanical, physical and barrier properties (light transmittance, WVP, TS, and EB) and inducing

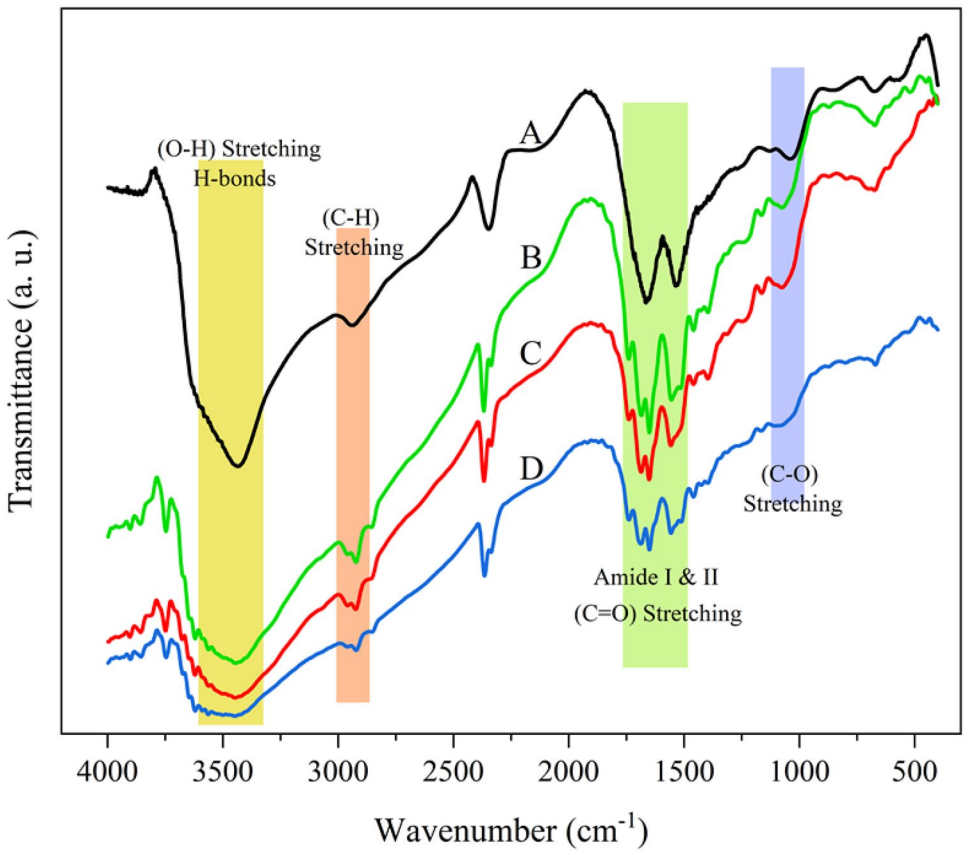

Fig. 3 FTIR spectra of SC film combined with ZnO NPs and REO. (a) (SC), (b) (SC/2%REO/1%ZnO NPs), (c) (SC/2%REO), (d) (SC/1%ZnO NPs)

remarkable antimicrobial activity. The SEM images and spectroscopic findings revealed that the ZnO NPs spread uniformly in the SC film matrix. These results propose that nanotechnology can enhance the application of biodegradable films for food packaging applications. We therefore recommend the fabricated, eco-friendly, nanocomposite films for use on an industrial scale.

Acknowledgements The authors are grateful to Maragheh University of Medical Sciences for funding this work.

Compliance with Ethical Standards

Conflict of interest The authors declare no conflict of interest.

References

1. Tankhiwale R, Bajpai SK (2012) Preparation, characterization and antibacterial applications of ZnO-nanoparticles coated polyethylene films for food packaging. Coll Surf B: Biointerfaces 90:16–20
2. Bagheri V, Ghanbarzadeh B, Ayaseh A, Ostadrahimi A, Ehsani A, Alizadeh-Sani M, Adun PA (2019) The optimization of physico-mechanical properties of bionanocomposite films based on gluten/carboxymethyl cellulose/cellulose nanofiber using response surface methodology. Poly Test 78:105989
3. Umamaheswari G, Sanuja S, John VA, Kanth SV, Umapathy MJ (2015) Preparation, characterization and anti-bacterial activity of zinc oxide-gelatin nanocomposite film for food packaging applications. Polym Polym Compos 23(3):199–204
4. Alizadeh-Sani M, Ehsani A, Kia EM, Khezerlou A (2019) Microbial gums: introducing a novel functional component of edible coatings and packaging. Appl Microbiol Biotechnol 103(17):6853–6866
5. Piñeros-Hernandez D, Medina-Jaramillo C, López-Córdoba A, Goyanes S (2017) Edible cassava starch films carrying rosemary antioxidant extracts for potential use as active food packaging. Food Hydrocoll 63:488–495
6. Alizadeh-Sani M, Mohammadian E, McClements DJ (2020) Eco-friendly active packaging consisting of nanostructured biopolymer matrix reinforced with TiO2 and essential oil: application for preservation of refrigerated meat. Food Chem. https://doi.org/10.1016/j.foodchem.2020.126782
7. Alizadeh-Sani M, Rhim J-W, Azizi-Lalabadi M, Hemmati-Dinarvand M, Ehsani A (2020) Preparation and characterization of functional sodium caseinate/guar gum/TiO2/cumin essential oil composite film. Int J Biol Macromol 145:835–844
8. Moghaddas Kia E, Ghasempour Z, Alizadeh M (2018) Fabrication of an eco-friendly antioxidant biocomposite: Zedo gum/sodium caseinate film by incorporating microalgae (Spirulina platensis). J Appl Polym Sci 135(13):46024
9. Fabra MJ, Talens P, Chiralt A (2008) Tensile properties and water vapor permeability of sodium caseinate films containing oleic acid–beeswax mixtures. J Food Eng 85(3):393–400
10. Suppakul P, Miltz J, Sonneveld K, Bigger SW (2003) Active Packaging technologies with an emphasis on antimicrobial packaging and its applications. J Food Sci 68(2):408–420
11. Fabra MJ, Talens P, Chiralt A (2009) Microstructure and optical properties of sodium caseinate films containing oleic acid–beeswax mixtures. Food Hydrocoll 23(3):676–683
12. Kia EM, Ghasempour Z, Ghanbari S, Pirmohammadi R, Ehsani A (2018) Development of probiotic yogurt by incorporation of milk protein concentrate (MPC) and microencapsulated Lactobacillus paracasei in gellan-caseinate mixture. Br Food J. https://doi.org/10.1108/BFJ-12-2017-0668
13. Sani MA, Ehsani A, Hashemi M (2017) Whey protein isolate/cellulose nanofibre/TiO2 nanoparticle/rosemary essential oil nanocomposite film: its effect on microbial and sensory quality of lamb meat and growth of common foodborne pathogenic bacteria during refrigeration. Int J Food Microbiol 251:8–14
14. Ojeda-Sana AM, van Baren CM, Elechosa MA, Juárez MA, Moreno S (2013) New insights into antibacterial and antioxidant activities of rosemary essential oils and their main components. Food cont 31(1):189–195
15. Li K-K, Yin S-W, Yang X-Q, Tang C-H, Wei Z-H (2012) Fabrication and characterization of novel antimicrobial films derived from thymol-loaded zein–sodium caseinate (SC) nanoparticles. J Agricul Food Chem 60(46):11592–11600
16. Al-Naamani L, Dobretsov S, Dutta J (2016) Chitosan-zinc oxide nanoparticle composite coating for active food packaging applications. Innovat Food Sci Emerg Technol 38:231–237
17. Alizadeh-Sani M, Khezerlou A, Ehsani A (2018) Fabrication and characterization of the bionanocomposite film based on whey protein biopolymer loaded with TiO2 nanoparticles, cellulose nanofibers and rosemary essential oil. Indust Crops Prod 124:300–315
18. ASTM-D1746-09 (1977) Annual Book of ASTM. American Society for Testing and Materials, Philadelphia, PA
19. ASTM-E96 (1995) Annual Book of ASTM. American Society for Testing and Materials, Philadelphia, PA
20. Alswat AA, Ahmad MB, Saleh TA, Hussein MZB, Ibrahim NA (2016) Effect of zinc oxide amounts on the properties and antibacterial activities of zeolite/zinc oxide nanocomposite. Mater Sci Eng: C 68:505–511
21. Luo Z, Qin Y, Ye Q (2015) Effect of nano-TiO2-LDPE packaging on microbiological and physicochemical quality of Pacific white shrimp during chilled storage. Int J Food Sci Technol 50(7):1567–1573
22. Alizadeh-Sani M, Hamishehkar H, Khezerlou A, Maleki M, Azizi-Lalabadi M, Bagheri V, Safaei P, Azimi T, Hashemi M, Ehsani A (2020) Kinetics analysis and susceptibility coefficient of the pathogenic bacteria by titanium dioxide and zinc oxide nanoparticles. Adv Pharmac Bull 10(1):56
23. Ando H, Kawasaki N, Yamano N, Uegaki K, Nakayama A (2015) Biodegradation of a poly (ε-caprolactone-co-l-lactide)–visible-light-sensitive TiO2 composite with an on/off biodegradation function. Polym Degrad Stabil 114:65–71
24. Azizi-Lalabadi M, Ehsani A, Alizadeh-Sani M, Khezerlou A, Mirzanajafi-Zanjani M, Divband B, Zolfaghari H, Bagheri V (2019) Nanoparticles and zeolites: antibacterial effects and their mechanism against pathogens. Curr Pharmac Biotechnol 20(13):1074–1086
25. Choi WS, Singh S, Lee YS (2016) Characterization of edible film containing essential oils in hydroxypropyl methylcellulose and its effect on quality attributes of 'Formosa'plum (Prunus salicina L.). LWT-Food Science and Technology 70:213–222
26. Arfat YA, Benjakul S, Prodpran T, Sumpavapol P, Songtipya P (2014) Properties and antimicrobial activity of fish protein isolate/fish skin gelatin film containing basil leaf essential oil and zinc oxide nanoparticles. Food Hydrocoll 41:265–273
27. Alebooyeh R, MohammadiNafchi A, Jokr M (2018) The effects of ZnOnanorodson the characteristics of sago starch biodegradable films. J Chem Health Risks 2(4)
28. Kuang Q, Xu J, Liang Y, Xie F, Tian F, Zhou S, Liu X (2017) Lamellar structure change of waxy corn starch during gelatinization by time-resolved synchrotron SAXS. Food Hydrocoll 62:43–48

29. Almasi H, Ghanbarzadeh B, Entezami AA (2010) Physicochemical properties of starch–CMC–nanoclay biodegradable films. Int J Biol Macromol 46(1):1–5
30. Zolfi M, Khodaiyan F, Mousavi M, Hashemi M (2014) Development and characterization of the kefiran-whey protein isolate-TiO2 nanocomposite films. Int J Biol Macromol 65:340–345
31. Zolfi M, Khodaiyan F, Mousavi M, Hashemi M (2014) The improvement of characteristics of biodegradable films made from kefiran–whey protein by nanoparticle incorporation. Carbohydr Polym 109:118–125
32. Hosseini SF, Rezaei M, Zandi M, Farahmandghavi F (2015) Fabrication of bio-nanocomposite films based on fish gelatin reinforced with chitosan nanoparticles. Food Hydrocoll 44:172–182
33. El-Wakil NA, Hassan EA, Abou-Zeid RE, Dufresne A (2015) Development of wheat gluten/nanocellulose/titanium dioxide nanocomposites for active food packaging. Carbohydr Polym 124:337–346
34. Zhang Y, Niu Y, Luo Y, Ge M, Yang T, Yu LL, Wang Q (2014) Fabrication, characterization and antimicrobial activities of thymol-loaded zein nanoparticles stabilized by sodium caseinate–chitosan hydrochloride double layers. Food Chem 142:269–275
35. Wang L-J, Yin Y-C, Yin S-W, Yang X-Q, Shi W-J, Tang C-H, Wang J-M (2013) Development of novel zein-sodium caseinate nanoparticle (ZP)-stabilized emulsion films for improved water barrier properties via emulsion/solvent evaporation. J Agricul Food Chem 61(46):11089–11097
36. Pereda M, Amica G, Rácz I, Marcovich NE (2011) Structure and properties of nanocomposite films based on sodium caseinate and nanocellulose fibers. J Food Eng 103(1):76–83
37. Rouhi J, Mahmud S, Naderi N, Ooi CR, Mahmood MR (2013) Physical properties of fish gelatin-based bio-nanocomposite films incorporated with ZnO nanorods. Nanoscale Res Lett 8(1):364
38. Zhou J, Wang S, Gunasekaran S (2009) Preparation and characterization of whey protein film incorporated with TiO2 nanoparticles. J Food Sci 74(7):N50–N56
39. Zhou J, Wang S, Gunasekaran S (2009) Preparation and characterization of whey protein film incorporated with TiO_2 nanoparticles. J Food Sci 74(7)
40. Li Y, Jiang Y, Liu F, Ren F, Zhao G, Leng X (2011) Fabrication and characterization of TiO 2/whey protein isolate nanocomposite film. Food Hydrocoll 25(5):1098–1104
41. Zolfi M, Khodaiyan F, Mousavi M, Hashemi M (2014) Development and characterization of the kefiran-whey protein isolate-TiO 2 nanocomposite films. Int J Biol Macromol 65:340–345
42. Mergler Y, Schaake R (2004) Relation between strain hardening and wear resistance of polymers. J Appl Polym Sci 92(4):2689–2692
43. Sun L, Gibson RF, Gordaninejad F, Suhr J (2009) Energy absorption capability of nanocomposites: a review. Compos Sci Technol 69(14):2392–2409
44. Todorov L, Viana J (2007) Characterization of PET nanocomposites produced by different melt-based production methods. J Appl Polym Sci 106(3):1659–1669
45. Limpisophon K, Tanaka M, Osako K (2010) Characterisation of gelatin–fatty acid emulsion films based on blue shark (Prionace glauca) skin gelatin. Food Chem 122(4):1095–1101
46. Tongnuanchan P, Benjakul S, Prodpran T (2013) Physico-chemical properties, morphology and antioxidant activity of film from fish skin gelatin incorporated with root essential oils. J Food Eng 117(3):350–360
47. Yamada T, Hao L, Tada K, Konagaya S, Li G (2006) Crystallization characteristics of PET/TiO2 nanocomposites. Mater Scie 2:154–160
48. Shankar S, Teng X, Li G, Rhim J-W (2015) Preparation, characterization, and antimicrobial activity of gelatin/ZnO nanocomposite films. Food Hydrocoll 45:264–271
49. Mohanapriya S, Mumjitha M, Purnasai K, Raj V (2016) Fabrication and characterization of poly (vinyl alcohol)-TiO2 nanocomposite films for orthopedic applications. Journal of the mechanical behavior of biomedical materials 63:141–156
50. Muyonga J, Cole C, Duodu K (2004) Characterisation of acid soluble collagen from skins of young and adult Nile perch (Lates niloticus). Food Chem 85(1):81–89
51. Nikoo M, Xu X, Benjakul S, Xu G, Ramirez-Suarez JC, Ehsani A, Kasankala LM, Duan X, Abbas S, (2011) Characterization of gelatin from the skin of farmed Amur sturgeon Acipenser schrenckii. Int Aquat Res (Islamic Azad University, Tonekabon Branch) 3(2)